Corrosion Science xxx (xxxx) xxx–xxx

Contents lists available at ScienceDirect

Corrosion Science

journal homepage: www.elsevier.com/locate/corsci

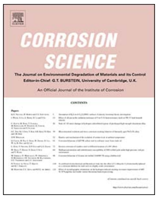

The corrosion of $Zr(Fe, Cr)_2$ and Zr_2Fe secondary phase particles in Zircaloy-4 under 350 °C pressurised water conditions

Kirsty Annand[a,*], Magnus Nord[a], Ian MacLaren[a], Mhairi Gass[b]

[a] *Materials and Condensed Matter Physics, School of Physics and Astronomy, University of Glasgow, Glasgow G12 8QQ, UK*
[b] *AMEC Foster Wheeler, Clean Energy, Walton House, Birchwood Park, WA3 6GA, UK*

ARTICLE INFO

Keywords:
Oxidation
SPPs
Zircaloy-4
STEM
DualEELS

ABSTRACT

Using Scanning Transmission Electron Microscopy (STEM) coupled with Dual Electron Energy Loss Spectroscopy (DualEELS) and scanned diffraction, the corrosion and incorporation of Secondary Phase Particles (SPPs) in the oxide layer of Zircaloy-4 material has been investigated. This study focuses on mapping the corrosion of Zr_2Fe and $Zr(Fe, Cr)_2$ precipitates during the oxidation process and depicting their morphology as the oxidation front advances through the material. It has been found that Zr_2Fe SPPs retain the same general shape as in their pre oxidation stage, and transform to a nanocrystalline homogeneous mixed oxide, with a strong crystallographic texture, but hitherto unknown structure. The $Zr(Fe, Cr)_2$ Laves-phase SPPs however, oxidise in a notably more complicated manner. As the α-Zr around an SPP begins to oxidise, the SPP is completely encapsulated by the ZrO_2 whilst much of the SPP remains initially unoxidised. But, on oxidation, significant elemental segregation takes place, usually leaving a Cr_2O_3-rich cap, a nanocrystalline Zr,Cr mixed oxide body and veins of well-crystallised metallic iron. Both forms of SPP have a different expansion on oxidation compared to the Zr, resulting in cracking of the ZrO_2.

1. Introduction

Worldwide, Zircaloy-4 (Zr-1.5%Sn-0.2%Fe-0.1%Cr) has been a popular material of choice for the containment of nuclear fuel and other structural components within commercial Pressurised Water Reactors (PWRs), due to their high corrosion resistance [1], low thermal neutron cross section [2], superior mechanical properties, and favourable chemical stability in highly aggressive environments. However, waterside corrosion of these cladding materials results in the creation of an oxide layer on the surface of the metal, resulting in degradation of their integrity over time. It is well established that the corrosion process of zirconium base alloys is a multifaceted one, characterised by an initial, rapid formation of a thin oxide layer on the surface of the material; followed by a decreased oxidation rate which follows the square or cube root of time [1,3], up until 2–4 μm of oxide has grown on the surface of the metal. Following this, a kinetic transition occurs and the oxidation proceeds more rapidly again. This process is periodic, and may be repeated several times, until the oxide thickness grows almost linearly with time [1]. A number of recent studies have elucidated the nanoscale details of this process in the alpha-Zr phase in the Zircaloy [4–6]. In this case, with the addition of alloying elements such as Sn, Fe and Cr to the Zr base metal, up to a value of about 2 wt.%, the corrosion behaviour of the alloy becomes more predictable and less likely to suffer catastrophic breakaway corrosion. The Fe and Cr alloying elements are shown to have a solubility of < 150 wt. ppm in Zr-1.4% Sn [7], and 290 wt. ppm [8] in Zircaloy-4. Therefore, much of the content of these elements precipitate during the alpha-phase annealing as intermetallic-Zr compounds, which sit as precipitates within the base metal [1]. It should be noted that improved corrosion resistance with the addition of alloying elements is not always the case, such as is seen in some binary alloy systems. Although the addition of Cr to a Zr base alloy improves the alloy's resistance to oxidation [9], this improvement is offset by the fact that the introduction of $ZrCr_2$ laves phase precipitates to the matrix can result in embrittlement of the material [9]. In the Zr-Fe alloy system, the laves C15-Fe_2Zr phase is found to be the most stable phase [10], although others (such as c-$FeZr_2$), relatively less so [10]. Precipitates in the Zr1%Fe system have also been seen to show an increased oxidation rate when in contact with the gas:oxide surface [11].

There are two primary types of SPP which are found within Zircaloy alloy series, namely $Zr_2(Ni, Fe)$ and $Zr(Fe, Cr)_2$ type precipitates. The former is an intermetallic C16 phase (isostructural with $CuAl_2$), frequently seen in Zircaloy-2 [12–15], whereas the latter mostly appears as an hexagonal intermetallic Laves phase with the C14 structure, and is seen frequently in both Zircaloy-2 and -4 [12,13,15–20].

---

[*] Corresponding author.
E-mail address: k.annand.1@research.gla.ac.uk (K. Annand).

http://dx.doi.org/10.1016/j.corsci.2017.09.014
Received 6 January 2017; Received in revised form 1 September 2017; Accepted 11 September 2017
0010-938X/

Please cite this article as: Annand, K., Corrosion Science (2017), http://dx.doi.org/10.1016/j.corsci.2017.09.014

Early work by Chemelle et al. [12] aimed to investigate the morphology and composition of SPPs in Zircaloy-2, using transmission electron microscopy (TEM). They found that all precipitates were either nickel-bearing with a tetragonal Zr_2Ni-type phase (where Ni is partly replaced by Fe), or chromium-bearing with a hexagonal $ZrCr_2$-type phase (where Cr is partly replaced by Fe). No iron-zirconium particles were detected. Later, Charquet [7] found that an increased iron content resulted in Zircaloy-4 having a better resistance to corrosion under steam conditions. However, the results reveal that in a Zr-1.4% Sn matrix, adding Fe in an amount equivalent to the (Fe + Cr) content in Zircaloy-4 is less effective than the simultaneous addition of Fe and Cr. Therefore, it was decided to study the influence of the Fe/Cr ratio in Zircaloy-4 material. It was deduced that the optimum corrosion resistance is obtained for Fe/Cr ratios in the range from 1.5 to 5. They noted that, for ratios less than 4, the only precipitates observed correspond to the $Zr(Fe, Cr)_2$ phase, in which the proportions of iron and chromium are comparable to their nominal concentrations. Moreover, for larger Fe/Cr ratios, further phases of the type Zr_2Fe and Zr_3Fe were found, highlighting that the substitution of Cr by Fe in $ZrCr_2$ is limited.

In order to better understand these SPPs, Meng et al. [13] then analysed them in Zircaloy-2 using TEM and energy dispersive X-ray spectroscopy (EDS). The most common were the $Zr_2(Fe,Ni)$-type which exhibited two size ranges, the larger ones being found at the α-Zr grain boundaries. They had a composition of $Zr_2(Fe_{0.4\text{-}0.5}Ni_{0.6\text{-}0.5})$, and a body-centred tetragonal structure, as expected for this composition. The smaller of these particles were found to be generally smaller than 1 μm and had an elliptical shape. The second SPP type found was the hexagonal $Zr(Fe, Cr)_2$ Laves phase with a composition of $Zr(Cr_{0.55\text{-}0.57}Fe_{0.45\text{-}0.43})_2$. These particles had a size similar to the smaller (< 1 μm) $Zr_2(Fe, Ni)$-type precipitates and exhibited the expected hexagonal C14 structure. These $Zr(Fe,Cr)_2$ SPPs were also regularly found to contain parallel stacking-faults. It should be noted that an SPP size of 1 μm is around 5 times larger than what would be expected in the largest SPPs in industrial alloys (of the order to 100–200 nm). As Zircaloy-2 has a different composition to Zircaloy-4, the corrosion resistance will differ between alloys, and thus, this reference may not be entirely adequate for comparison between SPP size in work by Meng et al. [13], and the current study.

Literature suggests that the oxidation process is considerably altered when factors such as distribution, size and chemical composition of the $Zr(Fe, Cr)_2$ intermetallic precipitates in Zircaloy-2 and Zircaloy-4 and $Zr_2(Fe,Ni)$ particles in Zircaloy-2 [17], are varied. However, there are still many outstanding questions about the exact mechanisms by which the oxidation of SPPs takes place. It is understood that the corrosion resistance of the alloy is strongly dependant on microstructure with the composition, size and volume fraction of SPPs being of particular importance. Optimal balance of these properties allows for fine control of life-limiting properties of the alloy such as corrosion resistance, hydrogen pick up and grain size [21]. In particular, it has been noted that favourable nodular corrosion resistance requires fine precipitates [22], whereas a certain minimum particle size is necessary for satisfactory uniform corrosion behaviour [23].

The oxidation of the Laves phase precipitates has been studied previously using conventional TEM and spot analysis with EDS. Pêcheur et al. [17] showed after oxidation in steam at 400 °C that such precipitates in Zircaloy 4 are often oxidised after the surrounding Zr matrix is oxidised to ZrO_2, that some diffraction patterns from oxidised SPPs could be consistent with a tetragonal ZrO_2 phase, and that some iron was redistributed as bcc metallic iron within the oxidised particles. De Gabory *et al.* [20] also recently concluded that the oxidation of such C14 Laves phase precipitates results in nanocrystalline areas with a large phase content of tetragonal ZrO_2. Pêcheur [24] studied the oxidation of similar precipitates in Zircaloy-4 in superheated lithiated water. They found that it is not until ~300 nm from the metal-oxide interface that SPPs begin to oxidise, and iron depletion is observed. It is suggested that due to the dissolution of iron from the precipitates to the surrounding zirconia matrix at this point, the alloying elements can modify the inner oxide grain properties, such as stabilising the tetragonal ZrO_2 phase.

There are also reports in Zr-1%Fe alloys of iron oxide precipitates in the oxide [11], although their structure was not determined, and there was no quantification of their exact composition. There are, however, very few observations of Zr_2Fe precipitates in Zircaloy-4 [25] and no known studies of the oxidation of such particles.

The current work is a systematic study of the structure and chemistry of SPPs in Zircaloy-4 after corrosion in pressurised water at 360 °C covering both Zr_2Fe and $Zr(Fe, Cr)_2$ type precipitates. Specifically, mapping of the chemistry using electron energy loss spectroscopy (EELS) spectrum imaging using DualEELS is used to produce spatially resolved quantitative maps of elemental content with few nanometre resolution elucidating in detail the oxidation process. This is combined with scanned diffraction to elucidate the crystallographic structure within these nanocrystalline oxidised SPPs. It is shown that whilst the oxidation of Zr_2Fe is relatively straightforward, the oxidation of the Laves phase precipitates is highly complex resulting in segregation into bands of a mixed Cr-Zr oxide and well-crystallised α-Fe.

2. Experimental methods

2.1. Materials and corrosion

All samples were prepared and corroded by Amec Foster Wheeler. The material of interest is standard recrystallised annealed (RXA) Zircaloy-4 (Zr-1.5%Sn-0.2%Fe-0.1%Cr). Samples were mechanically polished to remove surface scratches before being pickled in an HF solution to remove 50 μm of material from all surfaces. The samples were then exposed to pressurised water at 180 bar and 350 °C with a room temperature pH of 10 for various durations to simulate PWR in-reactor conditions [26,27]. The average dissolved hydrogen content was measured to be 3.65 ppm using a calibrated hydrogen orbisphere. Oxide thicknesses were average thicknesses, as inferred from weight gain measurements using the relationship 15 mg/dm2 = 1 μm.

2.2. Microscopy

Using a FEI Nova Nanolab instrument, samples were lifted out as cross sections through the oxide. Protection of the sample surface was done using electron beam, and then ion beam deposited platinum before initial thinning with 30 kV Gallium ions was performed. Samples were then lifted out and attached to suitable copper support grids with platinum, and final thinning was performed using lower energy Ga beams down to 5 kV.

Scanning transmission electron microscopy (STEM) and EELS-spectrum imaging (EELS-SI) using a probe corrected JEOL ARM200F (cold FEG) with a GIF Quantum ER electron energy loss spectrometer with DualEELS functionality. Typically, a probe semiconvergence angle of 29 mrad was employed for EELS-SI acquisition and a post-specimen lens setup that gave a spectrometer acceptance angle of 36 ± 0.4 mrad. Step sizes for EELS-SI were typically a few nm.

In order to determine crystallographic information of the particles, scanned diffraction was performed with the same instrument using aberration-corrected Lorentz-mode (i.e. objective lens switched off, and the probe formed using the condenser lenses and the aberration corrector, with a small convergence angle) [28]. Acquisition of the scanned diffraction datasets was controlled using the Diffraction Imaging plug-in for Spectrum Imaging within Gatan Digital Micrograph. Datasets for Zr_2Fe and $Zr(Fe, Cr)_2$-type SPPs in the oxide were acquired using the 30 μm condenser lens aperture which gives a convergence angle of 1.5 mrad and a diffraction-limited probe size of ~0.8 nm, a 40 cm camera length to give the appropriate size of diffraction pattern on the Gatan Orius CCD camera, and a 0.5 s exposure time per pixel for the $Zr(Fe, Cr)_2$ dataset, and a 0.2 s exposure time per pixel for the Zr_2Fe dataset.